Photosynth Res (2012) 111:193–204
DOI 10.1007/s11120-011-9670-0

REGULAR PAPER

Self-assembly and energy transfer in artificial light-harvesting complexes of bacteriochlorophyll *c* with astaxanthin

J. Alster · T. Polívka · J. B. Arellano · P. Hříbek · F. Vácha · J. Hála · J. Pšenčík

Received: 4 February 2011 / Accepted: 2 July 2011 / Published online: 11 August 2011

Abstract Chlorosomes, the light-harvesting antennae of green photosynthetic bacteria, are based on large aggregates of bacteriochlorophyll molecules. Aggregates with similar properties to those in chlorosomes can also be prepared in vitro. Several agents were shown to induce aggregation of bacteriochlorophyll *c* in aqueous environments, including certain lipids, carotenes, and quinones. A key distinguishing feature of bacteriochlorophyll *c* aggregates, both in vitro and in chlorosomes, is a large (>60 nm) red shift of their Q_y absorption band compared with that of the monomers. In this study, we investigate the self-assembly of bacteriochlorophyll *c* with the xanthophyll astaxanthin, which leads to the formation of a new type of complexes. Our results indicate that, due to its specific structure, astaxanthin molecules competes with bacteriochlorophylls for the bonds involved in the aggregation, thus preventing the formation of any significant red shift compared with pure bacteriochlorophyll *c* in aqueous buffer. A strong interaction between both the types of pigments in the developed assemblies, is manifested by a rather efficient (~40%) excitation energy transfer from astaxanthin to bacteriochlorophyll *c*, as revealed by fluorescence excitation spectroscopy. Results of transient absorption spectroscopy show that the energy transfer is very fast (<500 fs) and proceeds through the S_2 state of astaxanthin.

Keywords Light-harvesting · Chlorosomes · Self-assembly · Bacteriochlorophyll aggregates · Astaxanthin

Introduction

Chlorosomes of green photosynthetic bacteria (Blankenship and Matsuura 2003; Frigaard and Bryant 2006) contain large aggregates of bacteriochlorophyll (BChl) *c*, *d* or *e* molecules arranged into curved lamellar structures (Psencik et al. 2004, 2006, 2009; Oostergetel et al. 2007, 2010; Ganapathy et al. 2009). The BChl aggregates are held together by interactions between the central Mg ion of one BChl molecule, a hydroxyl group at $C3^1$ of another BChl, and a keto group at $C13^1$ of a third BChl molecule (Hildebrandt et al. 1994; Balaban 2005). The close interaction between BChl molecules leads to a strong exciton coupling which is manifested by a large red shift of the Q_y absorption band. Carotenoids and quinones are also present in the chlorosomes, occupying the hydrophobic space between the lamellar layers of BChls (Psencik et al. 2006). Carotenoids in chlorosomes are involved in both light-harvesting and photoprotection (Melo et al. 2000; Psencik et al. 2002; Polivka and Frank 2010); whereas quinones

Electronic supplementary material The online version of this article (doi:10.1007/s11120-011-9670-0) contains supplementary material, which is available to authorized users.

J. Alster · J. Hála · J. Pšenčík (✉)
Faculty of Mathematics and Physics, Charles University, Ke Karlovu 3, 121 16 Praha, Czech Republic
e-mail: psencik@karlov.mff.cuni.cz

T. Polívka · P. Hříbek · F. Vácha · J. Pšenčík
Institute of Physical Biology, University of South Bohemia, Zámek 136, 373 33 Nové Hrady, Czech Republic

T. Polívka · F. Vácha
Biology Centre, Academy of Sciences of the Czech Republic, Branišovská 31, 370 05 České Budějovice, Czech Republic

J. B. Arellano
Instituto de Recursos Naturales y Agrobiología de Salamanca (IRNASA-CSIC), Apdo. 257, 37071 Salamanca, Spain

mediate a protective quenching of the excitation energy in chlorosomes of green sulfur bacteria in the presence of oxygen (Frigaard et al. 1997). A chlorosome envelope is thought to be formed by a monolayer of proteins and lipids (Sorensen et al. 2008); it covers all of the chlorosome surface except the region where the chlorosome is attached to the cytoplasmic membrane. On this side, the chlorosome is delimited by a paracrystalline baseplate composed of CsmA proteins, which bind BChl *a* and carotenoids (Sakuragi et al. 1999; Bryant et al. 2002; Montano et al. 2003; Pedersen et al. 2008).

Aggregates of chlorosomal BChls or their synthetic analogs can also be prepared in vitro, either in non-polar or polar environments (for reviews see Balaban et al. 2005; Miyatake and Tamiaki 2005; Miyatake and Tamiaki 2010). In polar environments, e.g., in aqueous solutions, the aggregation of BChl *c* is driven by hydrophobic interactions (Klinger et al. 2004; Zupcanova et al. 2008). Addition of a suitable non-polar component is necessary to induce aggregation, most likely because hydrophobic interactions between farnesyl tails of BChl *c* molecules alone are not sufficiently strong to drive it. Lipids are well-known to play such an inducing effect on BChl *c* aggregation (Hirota et al. 1992; Uehara et al. 1994; Steensgaard et al. 2000), but there are other molecules that also induce aggregation of BChl *c* in aqueous solutions, for example, quinones with a hydrophobic side-chain (Alster et al. 2008), or carotenes such as chlorobactene (Klinger et al. 2004), and β-carotene (Alster et al. 2010). Each of these additional components affects the properties of the formed assemblies in a distinct way. Aggregates with quinones exhibit redox-dependent quenching of the BChl *c* excitation (Alster et al. 2008), whereas, energy transfer from carotenoid to BChl *c* was observed in aggregates with β-carotene (Alster et al. 2010). The energy transfer proceeds mainly through the carotenoid S_2 state, i.e., in a manner similar to that in chlorosomes (Psencik et al. 2002), except that the efficiency of energy transfer in the aggregates ($\sim$30%) was lower than in chlorosomes (50–80%, (Melo et al. 2000; Psencik et al. 2002)).

In this contribution, properties of assemblies of BChl *c* with the xanthophyll astaxanthin were studied by steady-state and femtosecond time-resolved spectroscopy. As xanthophylls are not usually found in chlorosomes, we investigated whether they are able to induce aggregation of BChl *c*. Astaxanthin was chosen because it contains both a hydroxyl and a carbonyl group in each of its end rings, and they could have an effect on aggregation. In fact, the assemblies of BChl *c* with astaxanthin have unusual features when they are compared with all other successfully tested aggregation-inducing admixtures: astaxanthin does not induce any pronounced red shift of the BChl *c* Q_y band when they form assemblies, but it closely interacts with BChl *c* molecules. Compared with previously tested carotenoids, assemblies of BChl *c* with astaxanthin exhibit an improved absorption in the spectral range between 500 and 600 nm, where BChl *c* absorbs poorly. Additionally, astaxanthin is capable of transferring energy to BChl *c* in the assemblies. These properties make the assemblies interesting for potential use in artificial photosynthesis.

Materials and methods

Sample preparation

BChl *c* (Fig. 1a) was extracted from whole cells of the green sulfur bacterium *Chlorobaculum tepidum* (formerly known as *Chlorobium tepidum*), and purified by means of HPLC as described previously (Klinger et al. 2004). The four main homologs of BChl *c* were collected together, in the same ratio as they were isolated from chlorosomes. Astaxanthin (Fig. 1b) was purchased from Sigma and was used without further purification. Assemblies of BChl *c* with or without astaxanthin were prepared by mixing stock solutions of astaxanthin (in THF) and BChl *c* (in methanol), to reach several molar ratios of astaxanthin to BChl *c* within a range of 0.0–0.8 to 1.0. This mixture was then injected into stirred 50 mM Tris-HCl pH 8.0 buffer. The final concentration of BChl *c* and the percentage of organic solvents in the buffer were approximately 30 μM and <1% (v/v) for self-assembly experiments and 250 μM, and 3–4% (v/v) for transient absorption spectroscopy, respectively. Pigment concentrations were determined from absorption spectra, using the extinction coefficients of 70 mM^{-1} cm^{-1} for BChl *c* in methanol at the Q_y maximum (Stanier and Smith 1960) and 125 mM^{-1} cm^{-1} determined for the absorption maximum of astaxanthin in hexane (Weber 1988). Samples were left overnight in dark at room temperature to reach stable steady-state absorption spectra. Samples were gently homogenized in a water bath sonicator before measurement to avoid precipitates.

Optical spectroscopy

Steady-state absorption spectra were measured using a Specord 250 spectrophotometer (Analytic Jena). Absorption spectra were corrected for scattering by measuring the absorption spectra at two different distances from the detector. The difference spectra (Fig. S1) yielded the spectral profile of the light-scattering of the sample (Latimer and Eubanks 1962), which was also used for the calculation of correction curves for other samples of the same pigment composition. This approximation worked reasonably well even for samples with significantly different

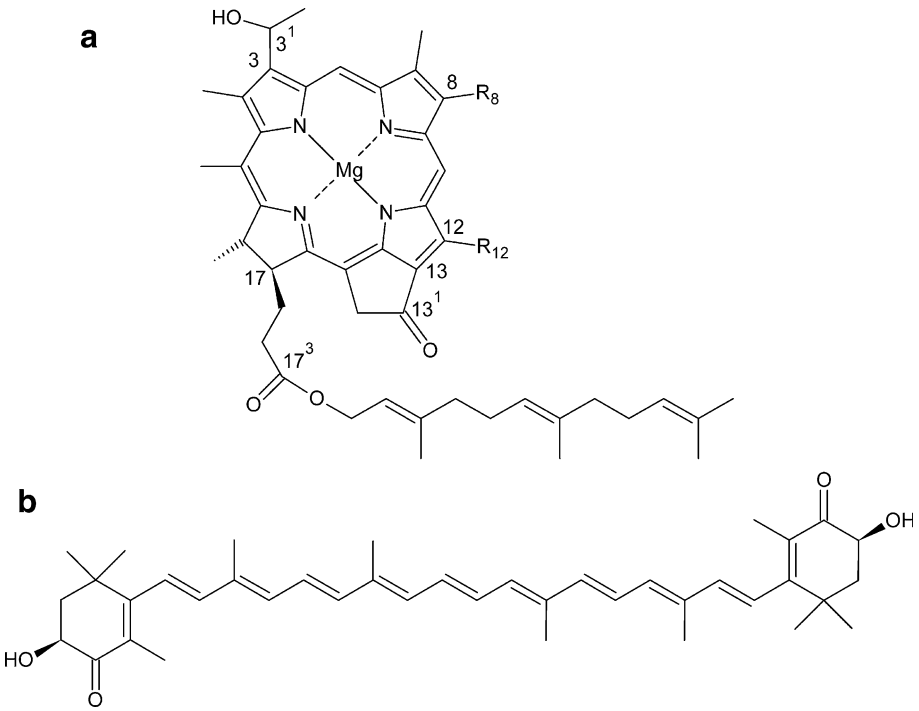

Fig. 1 Molecular structure of BChl *c* (**a**), and astaxanthin (**b**). Substituents of BChl *c* at R8 can be ethyl, propyl or isobutyl, at R12 methyl or ethyl. Astaxanthin is drawn as a (3*S*, 3′*S*) isomer

concentrations. The correction for a possible sieve effect was not performed.

Fluorescence excitation spectra were measured using a FluoroMax-2 fluorescence spectrometer (Jobin Yvon Spex). The fluorescence excitation spectra were corrected for the wavelength dependence of the excitation light intensity. The correction was done by measuring the intensity of the excitation light at the sample place by a calibrated diode power meter FieldMaster-GS (Coherent) with sensors LM-2-UV (in the region between 250 and 400 nm) and LM-2-VIS (400–800 nm). The second order of the excitation light and contribution of the stray light were attenuated using a 715 nm cut-off filter (Roper Scientific). The remaining contribution of the stray light above 715 nm was measured separately and subtracted from the excitation spectra. Optical density of the samples was adjusted to $\sim$0.15 at the Q_y maximum of BChl *c* to minimize the reabsorption of the emitted photons.

A set-up for femtosecond transient absorption measurements was based on an amplified laser system Integra-i (Quantronix), consisting of Er-fiber oscillator and Ti:Sapphire amplifier. It was used as a source of $\sim$120 fs pulses centered at 786 nm at a repetition rate of 1 kHz. Excitation pulses were obtained by directing a part of the amplifier output to the optical parametric amplifier (TOPAS, Light Conversion). A fraction of the 786 nm beam was focused to a 2 mm sapphire plate, where it generated broadband white-light pulses. The white-light pulses were further divided into the probe beam that overlapped with the excitation beam at the sample, and a reference beam. A spectrograph equipped with a double photodiode array (1024 elements) was used as a detector for both probe and reference beams. This arrangement allowed measurements of transient spectra in a spectral window of $\sim$240 nm. In all the measurements, the mutual polarization of the pump and the probe beams was set to the magic angle (54.7°), by placing a polarization rotator in the pump beam. Instrument response function was estimated, on the basis of the onset of instantaneous bleaching signal, to be Gaussian with the full width at half maximum of 150 fs. Sample was placed in a rotating cuvette consisting of two 1 mm quartz windows separated by a 1 mm Teflon spacer. Excitation intensities of $\sim 4 \times 10^{14}$ photons pulse^{-1} cm^{-2} (450–490 nm) and $\sim 10^{15}$ photons pulse^{-1} cm^{-2} (710 nm) were used. Steady-state absorption spectra were measured before and after the experiments to ensure that no degradation occurred during the data acquisition. Spectral bands did not change their shape during experiments, but overall decrease of the absorbance by about 5% occurred in some measurement. This is likely due to the precipitation, which is the consequence of the assembly formation and is further described in the Results.

Results

Self-assembly experiments

In contrast to other chlorophyll-like molecules, pure BChl *c* is partly soluble in aqueous buffer in a form with an

absorption spectrum basically identical to that of an anti-parallel piggy-back dimer, as determined by NMR in CH_2Cl_2 (Umetsu et al. 2003). This form is characterized by a Q_y absorption maximum between 710 and 715 nm, and two weaker peaks or shoulders at ~680 and ~635 nm, and is denoted as 'dimers' throughout this study.

Figure 2 compares the steady-state absorption spectra of pure BChl *c* in aqueous buffer (i.e. dimers) with those of BChl *c* assemblies with varying amounts of admixed astaxanthin. These spectra differ markedly from those of BChl *c* aggregates with lipids, carotenes or quinones, which were shown to induce aggregation of BChl *c* in aqueous solutions. The main difference is that astaxanthin does not induce any pronounced red shift of the BChl *c* Q_y band, instead the band remains at a position comparable with that of the BChl *c* dimers (~715 nm).

Like BChl *c*, astaxanthin is not freely soluble in aqueous buffer, but it can remain dispersed at low concentrations in buffer, if it is first dissolved in a small amount of THF, and then injected into the buffer in a way similar to the method used for the preparation of BChl *c* assemblies. Despite this, we can exclude that the BChl *c* assemblies with astaxanthin consist of a mixture of BChl *c* dimers and free astaxanthin dissolved in the buffer. The most compelling evidence of incorporation of astaxanthin into BChl *c* assemblies comes from the analysis of the astaxanthin-to-BChl *c* energy transfer (see below), but several other arguments arise from a closer inspection of the absorption spectra of the assemblies.

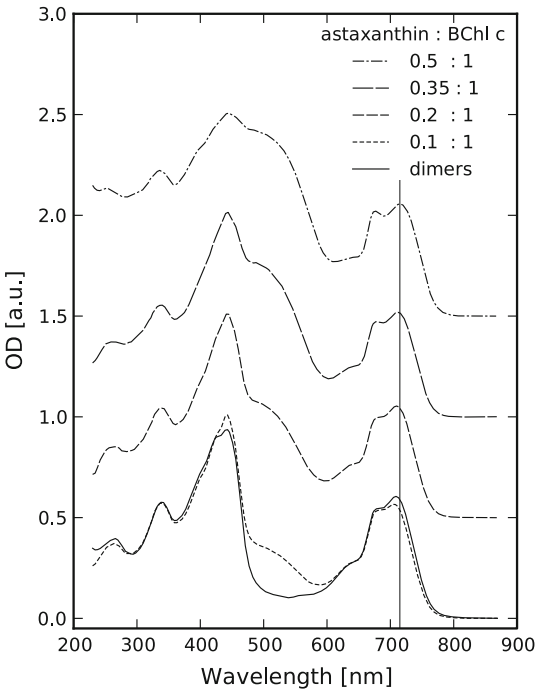

Fig. 2 Absorption spectra of BChl *c* assemblies with astaxanthin with different astaxanthin-to-BChl *c* molar ratios, corrected for light-scattering. Absorption spectrum of BChl *c* dimers (*solid line*) is shown for comparison. Spectra are normalized at 439 nm and offset by 0.5 a.u. to ease visualization. The vertical line is located at 715 nm to facilitate comparison

Firstly, although some precipitation occurs for any BChl *c* assembly with astaxanthin, it is significantly slower for samples with high pigment content containing both the BChl *c* and the astaxanthin than for the pure pigments dissolved in the buffer separately (i.e., BChl *c* and astaxanthin assemblies are soluble in aqueous buffer in higher concentrations than pure pigments). This cooperation is effective only up to a molar ratio of ~0.35:1 (astaxanthin-to-BChl *c*), which is the highest pigment molar ratio achieved without a significant precipitation. In addition, the assemblies of BChl *c* with astaxanthin exhibit slightly enhanced amplitude of the monomer-like BChl *c* absorption at ~675 nm compared with BChl *c* dimers, and its relative intensity increases with the astaxanthin concentration in the sample. It should be noted that monomeric bacteriochlorophyllide *c*, whose absorption spectrum is the same as that of BChl *c* (e.g. in methanol), is soluble in aqueous buffer and has its absorption maximum at 675 nm (Zupcanova et al. 2008). Therefore, it is expected that monomer-like BChl *c* in buffer would also have an absorption maximum at 675 nm. To emphasize the structural difference with aggregates of BChl *c* with lipids, carotenes or quinones, we call the formed complexes with astaxanthin 'assemblies' instead of 'aggregates'.

The formation of BChl *c*-astaxanthin assemblies also led to an increase of the light-scattering by the samples. For comparison with the fluorescence excitation spectra, and to determine the number of excited molecules at several wavelengths in the time resolved experiments, the correction of the absorption spectra for scattering was required (as described in Materials and Methods). As the absorption of BChl *c* in the Soret region overlaps with that of astaxanthin, it is not straightforward to determine the number of photons absorbed by each of the pigments in the BChl *c*-astaxanthin assemblies at a given wavelength. However, it can be done, if the absorption spectrum of the assemblies is compared with the one of the BChl *c* dimers and the contribution of the BChl *c* dimers is subtracted. Figure 3 shows the difference spectra between the absorption spectra of BChl *c*-astaxanthin assemblies with variable astaxanthin content and BChl *c* dimers. The difference spectra reflect the contribution of astaxanthin to each of the absorption spectra. A comparison of the difference spectra with the absorption spectrum of astaxanthin in THF (Fig. 3) shows that the main absorption peak of astaxanthin in assemblies is broader and shifted to longer wavelengths, similarly to what was observed in the artificial aggregates of BChl *c* with β-carotene and native chlorosomes (Arellano et al. 2000; Alster et al. 2010). In addition, the band at

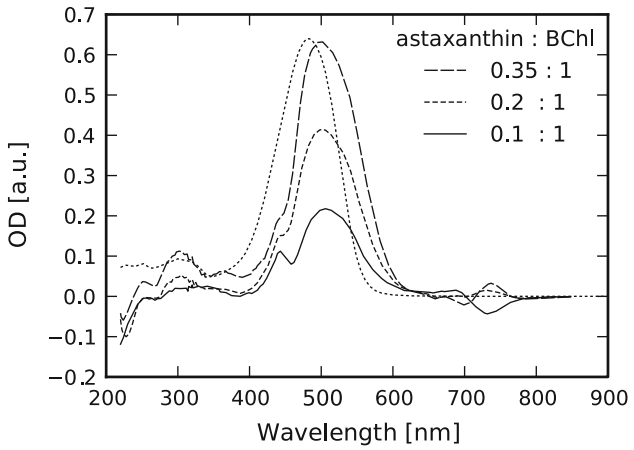

Fig. 3 Difference spectra between absorption of BChl *c* assemblies with astaxanthin and BChl *c* dimers, showing the contribution of astaxanthin to the absorption spectra of the assemblies. Spectra are compared with the absorption spectrum of astaxanthin in THF (*dotted line*)

~300 nm is more pronounced for astaxanthin in BChl *c* assemblies. Besides the contribution of astaxanthin to the difference spectrum, other minor contributions come from the changes in the Soret band (~400–450 nm) and Qy band (700–750 nm) of BChl *c* upon formation of the assemblies with astaxanthin.

Excitation spectra

Fluorescence excitation spectra were measured to determine whether astaxanthin in the assemblies was able to transfer excitation energy to BChl *c*. Figure 4 compares the

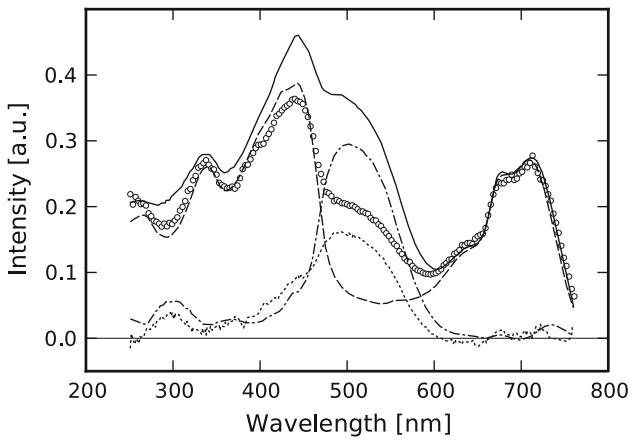

Fig. 4 Fluorescence excitation spectrum of BChl *c* assembly with astaxanthin (*circles*). The spectrum is compared with the absorption $(1 - T)$ spectra of BChl *c* assembly with astaxanthin (*solid line*) and BChl *c* dimers (*dashed line*). The difference spectrum between both absorption $(1 - T)$ spectra (*dash-dot line*), and the difference spectrum between the absorption $(1 - T)$ spectrum, and the excitation spectrum of BChl *c* assembly with astaxanthin (*dotted line*) are also shown

absorption $(1 - T)$ spectrum, corrected for the light-scattering, with the fluorescence excitation spectrum detected at 770 nm. Excitation spectrum exhibited clear features of the astaxanthin absorption (a pronounced shoulder at around 525 nm), clearly demonstrating that the excitation energy is transferred from astaxanthin to BChl *c*. The quantum efficiency of the transfer could be determined by comparison with the absorption $(1 - T)$ spectrum of BChl *c* dimers. The difference between the absorption $(1 - T)$ spectra of BChl *c* assemblies with astaxanthin and BChl *c* dimers reflected the total astaxanthin absorption in the sample (similarly as in Fig. 3). On the other hand, the difference spectrum between absorption and excitation spectrum of the BChl *c* assemblies with astaxanthin revealed the portion of the photons absorbed by astaxanthin and not transferred to BChl *c*. In Fig. 4, it can be clearly seen that the latter difference spectrum also resembles the astaxanthin absorption in the sample, including the band at 300 nm. The quantum efficiency of the energy transfer from astaxanthin to BChl *c* could be determined from these spectra. The assessment was complicated by the accompanying changes in the BChl *c* Soret band upon the formation of the assemblies, mainly in the spectral range between 400 and 450 nm. This contributed to a rather large uncertainty of the determined efficiency, which was found to be $40 \pm 7\%$, taking into account both measurement errors and precision of corrections.

Transient absorption

To determine the kinetics and pathways of the excitation energy transfer from astaxanthin, transient absorption spectra for the BChl *c* assemblies with astaxanthin were recorded. Additionally, the transient absorption spectra of samples without astaxanthin were measured for comparison and determination of the relaxation processes in BChl *c* not affected by the presence of astaxanthin. Unfortunately, BChl *c* dimers quickly precipitate after preparation at the concentration needed for transient absorption measurements. Therefore, a small amount of lecithin (≤0.1 mol/mol lecithin to BChl *c*) was added to the BChl *c*, dissolved in methanol before injection into the buffer, which prevented the (fast) precipitation of the sample, and led to a negligible shift of the Q_y absorption band compared with the BChl *c* dimers. This sample is hereafter referred to as BChl *c* dimers with lecithin.

Transient spectra were measured after excitation at three different excitation wavelengths: 450, 490, and 710 nm. Excitation at 710 nm was used to check whether, there was any significant exciton coupling between BChl *c* and astaxanthin. In such a case, transient changes in the region of astaxanthin photobleaching or stimulated emission (PB/SE) would be expected, even though at 710 nm only

BChl *c* is excited. Transient spectra of BChl *c* assemblies with astaxanthin differed only slightly from those of BChl *c* dimers with lecithin, by a shift of the PB/SE signal in the BChl *c* Q_y region, and a small negative signal between 450 and 600 nm (Fig. S2). Although this difference may be caused by excitonic interaction between the BChl *c* and the astaxanthin, it can also be easily explained by a change in the BChl–BChl excitonic interaction between the two samples. At the moment, we are not able to distinguish between the two possibilities.

In order to determine the pathway of the energy transfer from astaxanthin to BChl *c*, two excitation wavelengths were used: Soret band of BChl *c* was preferentially excited at 450 nm and astaxanthin at 490 nm. However, strictly speaking, both the pigments were excited at both wavelengths, but in a different ratio. Figure 5 shows the transient spectra of BChl *c* assemblies with astaxanthin (astaxanthin-to-BChl *c* molar ratio of 0.2:1) after excitation at 490 nm. Transient signal under ~550 nm reflects mainly PB/SE of the S_2 state of astaxanthin, while excited state absorption (ESA) of the astaxanthin S_1 state dominates between 550 and 700 nm, and PB/SE of the BChl *c* Q_y band above 700 nm. Similar results were also obtained for a sample with an astaxanthin-to-BChl *c* molar ratio of 0.35:1. The lifetimes reported further in the text are representative values for all samples under study.

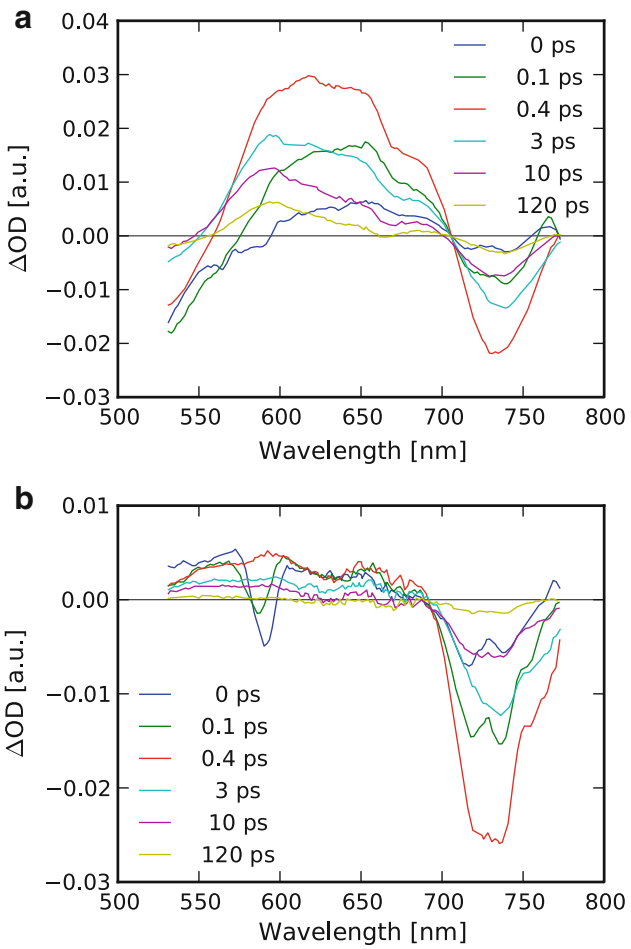

Fig. 5 Transient spectra of BChl *c*-astaxanthin assemblies after excitation at 490 nm (**a**). Transient spectra of BChl *c* dimers with lecithin after excitation at 490 nm (**b**); negative peak at 590 nm is Raman scattering of water. The spectra were smoothed by 10 point (±2.5 nm) adjacent averaging

Assuming multi-exponential relaxation, the data can be analyzed by a global analysis (van Stokkum et al. 2004), which provides rate constants and their pre-exponential factors for the whole wavelength range covered in the experiment (the decay associated spectra-DAS). This procedure reveals the most important relaxation processes occurring in the assemblies. However, this approach leads to a mixing of contributions from BChl *c* and astaxanthin states, which spectrally overlap and exhibit similar lifetimes. This complication can be avoided by separating the transient data into two parts: relaxation following excitation of astaxanthin, and BChl *c*, respectively (see Appendix). Subsequently, global analysis was performed on both the parts separately. As a consequence of the equations (A5), both the parts of transient data were normalized to the same number of absorbed photons.

The astaxanthin part of the transient data (Fig. 6a) retains almost the entire negative signal below 550 nm, most of the positive signal around 600 nm, and a part of the PB/SE of the BChl *c* Q_y band. The transient data revealed that the decrease in the transient absorption of the astaxanthin S_2 state (<550 nm), is connected with a concomitant rise of ESA signal around 620 nm (mainly from the astaxanthin S_1 state), and PB/SE signal in the Q_y region of BChl *c*. This process is reflected by the fastest component (~140 fs) obtained from a global analysis performed on the xanthophyll part of the transient data (Fig. 6c), clearly showing the energy transfer from the S_2 state of astaxanthin-to-BChl *c*.

The second fastest component has a lifetime of ~0.5 ps and an amplitude negative below ~600 nm, and positive between 600 and 700 nm. Such a lifetime and spectral profile are typical for vibrational relaxation within the S_1 state of carotenoids. For instance, the 0.6 ps component was attributed to the vibrational relaxation in the S_1 state of astaxanthin bound to α-crustacyanin (Ilagan et al. 2005). This and all other subsequent components also contain a minor contribution from the PB/SE of the BChl *c* Q_y band. The global analysis mainly reflects the relaxation of dominating components, (i.e., those of astaxanthin), and is not able to distinguish weaker components with similar lifetimes in the case of insufficient signal to noise ratio of the data. Therefore, more representative lifetimes for the decay of the BChl signal can be found in the BChl part of the transient data. Third component has a lifetime of 4.4 ps and corresponds to the main decay of the S_1 state of astaxanthin.

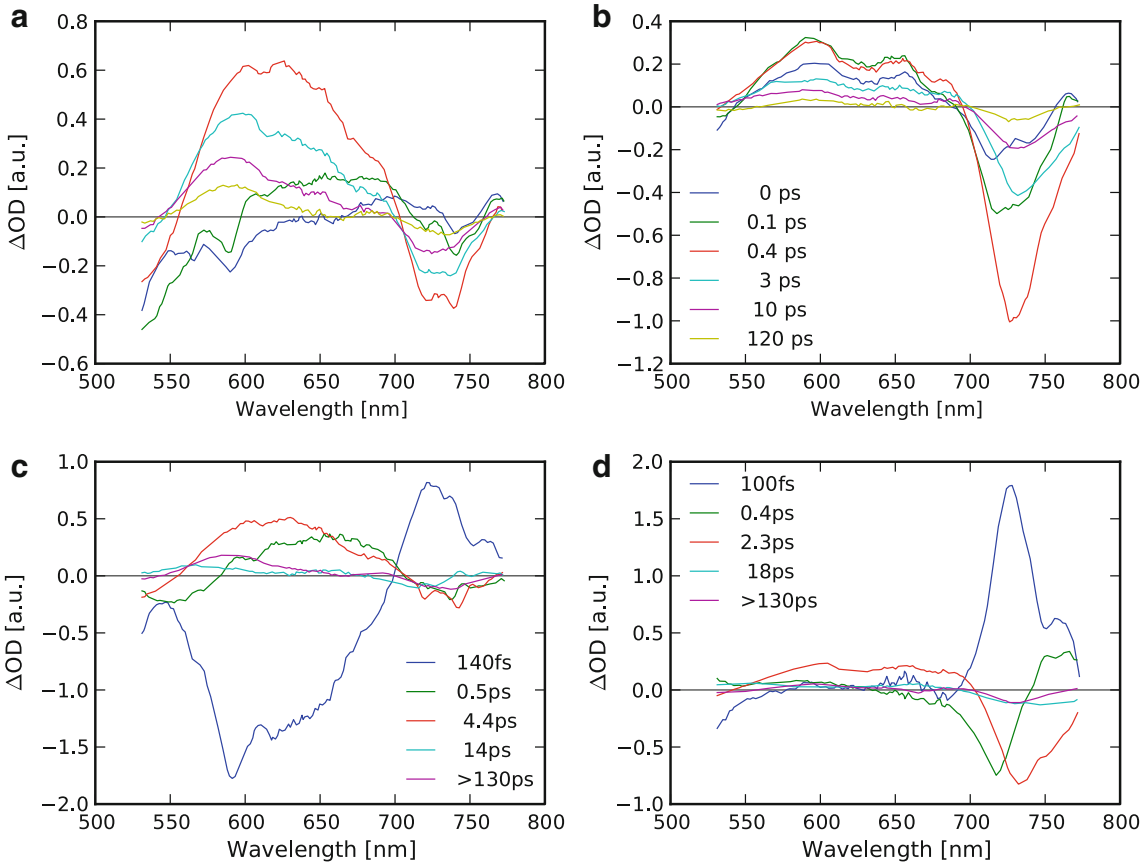

Fig. 6 Transient data of BChl *c* assemblies with astaxanthin with an astaxanthin-to-BChl *c* molar ratio of 0.2:1 after decomposition into a part corresponding to the excitation of astaxanthin (**a**—transient spectra, **c**—decay associated spectra) and BChl *c* (**b**—transient spectra, **d**—decay associated spectra). The color coding for **a** and **b** are the same. Arbitrary units for the panels **a** and **b** are also the same and so are they for panels **c** and **d**. The spectra were smoothed by 10 point (±2.5 nm) adjacent averaging

The next component, with a lifetime of ~14 ps, is dominated by a peak at 560 nm. A peak at similar position, although with a significantly shorter lifetime (1.9 ps) was observed for astaxanthin dissolved in carbon disulfide (Illagan et al. 2005), and it was suggested that the signal was due to either a S* state or excited state solvation. Though we observed much longer lifetime, it is worth noting that S* lifetime of 7 ps was measured in a water-soluble analog of astaxanthin, astalysine (Chabera et al. 2010), indicating that the S* lifetime may be sensitive to the environment. Consequently, we assigned the 14 ps component to the S* state of astaxanthin in the assemblies.

The last resolved component had a lifetime longer than the longest measured delay (130 ps), and corresponded with the relaxation of an ESA signal centered at 580 nm. This long-lived ESA signal is assigned to an astaxanthin triplet–triplet absorption based on comparison with previous results on aggregates of BChl *c* with *β*-carotene, where a similar signal was centered at 550 nm (Alster et al. 2010). This assignment was further supported by the observation of the triplet state of spheroidene and spheroidenone in reaction centers from *Rhodobacter sphaeroides* 2.4.1 and the mutant RCO2 (Arellano et al. 2004). The spheroidenone contains a keto group and shows a broader and red shifted triplet–triplet absorption spectrum compared with spheroidene, i.e., similar differences to those observed between *β*-carotene and astaxanthin.

The BChl *c* part of the transient data (Fig. 6b), on the other hand, retained most of PB/SE signal in the Q_y region of BChl *c* and some broad ESA signal between 550 and 680 nm. As expected, it is very similar to the transient signal of BChl *c* dimers with lecithin (Fig. 5b). This corroborates the relevance of the decomposition method. The only difference is found in a somewhat bigger amplitude of the broad ESA signal (550-700 nm), with a maximum around 610 nm in the BChl part of the transient data. Assuming no energy transfer from BChl *c* to astaxanthin (see below), this signal must have come from the xanthophyll contribution admixed to the BChl *c* part of the transient data during decomposition; this is most probably caused by small unavoidable errors in determining the populations of initially excited states.

It may be expected that the fastest relaxation process observed within the BChl *c* part of the transient data is internal conversion from the Soret to Q_y band. This process is connected with the fast increase of the SE signal of the BChl *c* Q_y band. It is also reflected as the fastest DAS component resolved by global analysis (Fig. 6d), with a lifetime of $\sim$100 fs. It should be stressed that this lifetime is shorter than the instrument response time; therefore, it is determined with rather a high uncertainty, and the spectral profile of this component most probably also contains some artifacts originating from coherent processes caused by excitation and/or the fact that the model used for global analysis does not account for a variable width of the instrument response function over the whole spectral region. Thus, the only conclusion we can draw is that the lifetime of internal conversion from the Soret to Q_y band is up to $\sim$100 fs.

The next two components revealed by global analysis have lifetimes of $\sim$0.4 ps, attributed to the energy redistribution in the BChl *c* Q_y band, and 2.4 ps, corresponding to the main decay of BChl *c*. The last two components, with lifetimes of 18 ps and >130 ps, are due to the relaxation of BChl *c* to the ultimate acceptor state of the assembly. We cannot exclude that the relaxation within the BChl *c* manifold is affected by annihilation, as observed for BChl aggregates in chlorosomes (Psencik et al. 2003). There is no signal which could be attributed to the energy transfer from BChl *c* to astaxanthin. This fact further supports an interpretation of the extraneous ESA around 610 nm in the BChl *c* part of the transient data as an artifact of the transient data decomposition.

Discussion

In previous studies, we have demonstrated that, in addition to lipids, specific carotenes and quinones induce aggregation of BChl *c* in aqueous buffers (Klinger et al. 2004; Alster et al. 2008, 2010). The aggregation is manifested by a red shift of the BChl *c* Q_y transition, which increases with the concentration of the aggregation-inducing species. However, the xanthophyll astaxanthin used in this study behaves differently. The red shift of the Q_y band of BChl *c* upon addition of astaxanthin is nearly absent, indicating that the assemblies of BChl *c* with astaxanthin are formed in a different manner. As the most plausible explanation, we propose that the hydroxyl group of the astaxanthin end ring (Fig. 1) competes for the Mg coordination with hydroxyl group of another BChl *c*. Similarly, keto oxygen of the astaxanthin end ring and BChl *c* (Fig. 1) may compete for hydrogen bonding with hydroxyl groups of both the pigments. However, at this stage, we do not have any direct evidence concerning the nature of interactions between astaxanthin and BChl *c*.

The suggested involvement of astaxanthin in the binding pattern thus prevents the stacking of many BChl *c* molecules, a prerequisite for their strong exciton coupling and, consequently, for the red shift of the BChl *c* Q_y band in the assemblies. It also explains the enhancement of the monomer-like peak in the absorption spectra, which certainly cannot originate from free monomers of BChl *c* in buffer. The interference of the astaxanthin functional groups with those involved in the aggregation of BChl *c* may be the reason why xanthophylls are not usually found in chlorosomes, although hydroxyl chlorobactene or OH-γ-carotene have been detected in minor amounts (<2% of total carotenoid content) in cells of some strains of *Chlorobaculum tepidum* (Takaichi et al. 1997). Chlorosomal carotenoids, e.g., chlorobactene, possess neither keto nor hydroxyl groups, and interact with BChl *c* mainly by hydrophobic and/or π–π interactions. The difference spectra between the BChl *c* assemblies with higher molar ratio of astaxanthin and BChl *c* dimers indicate the presence of some aggregates absorbing at around 740 nm (judging from the wave-like pattern in the Q_y band region; Fig. 3); however, most of the BChl *c* molecules exhibit spectral features of BChl *c* dimers. Although this means that the excitonic coupling between BChl *c* molecules is restricted to the level observed for dimers, the actual size of the BChl *c*-astaxanthin particles must be much larger, as judged by the increased scattering and precipitation. BChl *c*-astaxanthin assemblies thus consist mainly of excitonically coupled BChl *c* dimers interconnected with astaxanthin, and form particles, where these dimers are only interacting weakly.

Compelling evidence of energy transfer from astaxanthin-to-BChl *c*, with quantum efficiency of about 40%, was obtained by fluorescence excitation spectra. Further support comes from the global analysis of the transient data, which revealed a fast component of $\sim$140 fs, following the excitation of astaxanthin, with a spectral profile characteristic for energy transfer. This component indicates that the excitation absorbed by the S_2 state of astaxanthin (PB/SE below 550 nm) partly undergoes relaxation into the astaxanthin S_1 state (arrival of the energy reflected by a negative amplitude of this component between 550 and 700 nm which corresponds to a rise of ESA), and partly to BChl *c*, which is manifested by a positive amplitude above 700 nm (rise of PB/SE). In addition, the amplitudes of the transient data (PB/SE of the BChl *c* Q_y band) decomposed into parts following the excitation of astaxanthin and BChl *c* reflect the quantum efficiency of the astaxanthin to BChl *c* energy transfer, which is consistent with that determined by fluorescence excitation spectra.

Support for the suggested energy transfer pathway in the BChl *c* assemblies with astaxanthin can be found from the comparison of our transient data with some results derived from measurements of the S_1 and S_2 states lifetimes of astaxanthin in several solutions. Ilagan et al. (2005) determined the S_1 state lifetime of astaxanthin in methanol, acetonitrile, and carbon disulfide to be $\sim$5 ps, and the lifetime of S_2 state to be between 105 fs (methanol) and 165 fs (acetonitrile). Kopczynski et al. (2005) also reported a lifetime of $\sim$5 ps for the S_1 state of astaxanthin in various solutions ranging from toluene to methanol, and a lifetime of $\leq$120 fs for S_2 state of astaxanthin in acetone and dimethyl sulfoxide. The S_2 state relaxation was also measured by photon echo spectroscopy for astaxanthin in THF, and a lifetime of 160 fs was determined using the excitation pulses of $\sim$30 fs width (Christensson et al. 2009).

The lifetime of the S_1 state of astaxanthin in assemblies with BChl *c* was found to be 4.4 ps in this study. Such a small shortening of the S_1 state lifetime compared with the lifetime in solution is at the edge of reliability, yet, it may indicate a low efficiency S_1-mediated energy transfer pathway to BChl *c*. However, as there is no rise component in the BChl *c* PB/SE region matching the decay of astaxanthin S_1 state, we can safely conclude that S_1 pathway is closed in these assemblies, and all energy transfer proceeds through the S_2 route. This conclusion is also corroborated by the fact that carotenoids with effective conjugation length comparable with astaxanthin (e.g. lycopene or spirilloxanthin) have S_1 energy below 13,000 cm^{-1} (Billsten et al. 2002; Papagiannakis et al. 2003), thereby preventing the energy transfer to Q_y state of BChl *c* in the assemblies.

The S_2 state lifetime of astaxanthin, determined here, corresponds to the fastest component of the astaxanthin relaxation (140 fs). Since astaxanthin-to-BChl *c* energy transfer takes place in the assemblies, we must expect that the S_2 state lifetime of astaxanthin becomes shorter in assemblies compared with that in solution. Using the lifetime of 160 fs (Christensson et al. 2009), which fits within the uncertainty of 145 $\pm$ 50 fs obtained by Ilagan et al. (2005) in carbon disulfide, then, to ensure 40% efficiency determined by excitation spectra, the calculated energy transfer time is 240 fs. These values lead to the shortening of the S_2 state lifetime to $\sim$100 fs, which is shorter than the S_2 state lifetime in the presence of energy transfer determined by global analysis. However, the S_2 state lifetime is comparable with the instrument response time ($\sim$150 fs), and as such determined with rather a high uncertainty. On the other hand, the spectral shape of the 140 fs DAS component clearly indicates energy transfer to BChl *c*, and therefore the energy transfer observed in the excitation spectra certainly occurs from the S_2 state of astaxanthin, and the energy transfer time should be less than 500 fs. It should be noted that fixing the lifetime of this component to 100 fs does not affect DAS of this component, and the change of the residues is below the noise level.

The rather efficient and very fast energy transfer indicates that the BChl *c* and astaxanthin form assemblies with a close distance between both the pigments. This, together with other arguments reported in the "Results" section, excludes the possibility that our samples were just a mixture of dissolved BChl *c* and astaxanthin.

The lifetimes reported above were determined from the transient data decomposed into parts following the excitation of astaxanthin and BChl *c*, respectively, as described in the Results. It should be stressed that standard global analysis applied to non-separated transient data leads to very similar results, but the main advantage of the decomposition is the very illustrative analysis of the relaxation after excitation of either BChl *c* or astaxanthin.

The fast formation of the triplet state excludes its origin in intersystem crossing, and suggests singlet homofission similarly to the the BChl *c* aggregates with β-carotene (Alster et al. 2010). As described above, the S_1 lifetime of astaxanthin in the assemblies (4.4 ps) is slightly shorter than in solution ($\sim$5 ps). Since it was concluded that this shortening cannot be due to energy transfer to BChl *c*, it is possible to speculate that the shortening is caused by additional weak relaxation channel, leading to the triplet state formation by a singlet homofission mechanism with a quantum efficiency of $\sim$10%. Alternatively, the triplet state may be formed by the homofission from the S* state, which was detected in the assemblies studied here. Since the S* state is known to be a precursor of the homofission-generated triplet state in some proteins containing carotenoids (Gradinaru et al. 2001), it is feasible that the local environment of astaxanthin in the assemblies also provides favorable conditions for such pathway.

In conclusion, astaxanthin forms assemblies with BChl *c*, which exhibit rather an efficient and fast energy transfer from the S_2 state of astaxanthin to BChl *c*. Astaxanthin absorption in the assemblies covers mainly the spectral region between 450 and 600 nm, filling a substantial part of the gap between the Soret and Q_y band of BChl *c*. As the BChl *c* assemblies with astaxanthin are formed by self-assembly, their absorption covers a substantial part of the visible spectrum, and are relatively stable they might be an interesting model system for artificial light-harvesting systems.

Acknowledgments This study was supported by the Czech Ministry of Education, Youth and Sports (projects MSM0021620835, MSM6007665808, AV0Z50510513), Czech Science Foundation (projects 206/09/0375, 202/09/H041, 202/09/1330), and Spanish Ministry of Science and Innovation (AVCR-CSIC joint project 2008CZ0004). The authors would like to thank Ivana Hunalova,

Frantisek Matousek, and Anita Zupcanova for their help with pigment isolation.

Appendix: Transient data analysis

We assume simple kinetic model for excited state population N_i

$$\dot{N}_i(t) = \sum_i \left(-k_{ij}N_i(t) + k_{ji}N_j(t)\right) \quad (1)$$

where k_{ij} is the rate constant for energy/population transfer from one state i to the another state j and dot represents derivative with respect to time. By solving set of Eq. 1 (one for each state), and considering that each state contributes to transient signal proportionally to its population, we get the following model for describing transient absorption data

$$\Delta A(t) = \sum_j \left(\sum_i K_{ji}\varepsilon_i N_i(0)\right) \exp(-k_j t) \quad (2)$$

where indices i and j iterates over all energy states present in the sample, k_j is the overall rate constant of the state j ($k_j = \sum_i k_{ij}$), ε is a spectral profile associated with the given state, and coefficients K_{ij} describe the energy transfer between states, typically $K_{ij} = \frac{k_{ij}}{k_j - k_i}$ or product of similar terms. We can then perform global fitting analysis to find the overall rate constants and corresponding pre-exponential factors (i.e. the DAS)

$$\Delta A(t) = \sum_j DAS_j \exp(-k_j t) \quad (3)$$

Let's assume in accordance with the multi-exponential model that relaxation pathways from an excited state are the same regardless of its population. This is of course an approximation, because relaxation within the BChl *c* manifold is likely to be influenced by singlet–singlet annihilation, which the model does not describe. It follows that the transient signal consists of parts proportional to the initial population of states directly excited by pump pulse (the other way of summation in Eq. 2)

$$\Delta A(t) = \sum_i \left(\varepsilon_i \sum_j K_{ji} \exp(-k_j t)\right) N_i(0) = \sum_i \Delta a_i N_i(0) \quad (4)$$

If we perform at least P measurements with different and known ratio of the initial population of the excited states, where P is the number of the initially excited states (with non-zero $N_i(0)$), then we can determine the parts of the transient data corresponding to the relaxation from each of the initially excited states (Δa_i in Eq. 4). Note that these parts should be the same in all measurements, except that their weights $N_i(0)$ differ. Here we assume that only the S_2 state of astaxanthin and Soret band of BChl *c* are directly excited, and that the transient data separates into two parts: relaxation following excitation of astaxanthin, and BChl *c*, respectively. Therefore, we need to perform two transient absorption measurements with a different ratio between initial populations of the S_2 state of astaxanthin and the Soret band of BChl *c*. One theoretically possible way to change the excited state population is to use one excitation wavelength and two samples with different astaxanthin-to-BChl *c* molar ratios. However, different sample composition in this case results in a different way of assembly, and therefore, in different absorption spectra, breaking the condition that relaxation from excited state is the same. The other way is to use one sample and two different excitation wavelengths (close enough to excite the same electronic transitions and far enough to achieve significant change of excited populations ratio). In this case, we populate different parts from the inhomogeneously broadened electronic transition peaks; however, this should not influence the relaxation from the higher excited state significantly. We measured the transient data after excitation at two different wavelengths, 450 and 490 nm. Therefore, we can rewrite Eq. 4 describing the global decay at two excitation wavelength as

$$\begin{aligned}\Delta A_{450} &= \Delta a_{\mathrm{BChl}} N_{450}^{\mathrm{BChl}}(0) + \Delta a_{\mathrm{Car}} N_{450}^{\mathrm{Car}}(0)\\ \Delta A_{490} &= \Delta a_{\mathrm{BChl}} N_{490}^{\mathrm{BChl}}(0) + \Delta a_{\mathrm{Car}} N_{490}^{\mathrm{Car}}(0)\end{aligned} \quad (5)$$

where ΔA_{450} and ΔA_{490} represent transient data after excitation at 450 and 490 nm, respectively.

The initial excited state populations $N_\lambda^{\mathrm{molecule}}(0)$ could be determined directly from steady-state absorption spectra corrected for scattering, and energy in the pump pulse. From the two equations, two unknown matrices Δa_{BChl} and Δa_{Car}, which represent BChl *c* and astaxanthin part of the transient data, could be calculated (Fig. 6).

References

Alster J, Zupcanova A, Vacha F, Psencik J (2008) Effect of quinones on formation and properties of bacteriochlorophyll *c* aggregates. Photosynth Res 95:183–189

Alster J, Polivka T, Arellano JB, Chabera P, Vacha F, Psencik J (2010) beta-Carotene to bacteriochlorophyll *c* energy transfer in self-assembled aggregates mimicking chlorosomes. Chem Phys 373:90–97

Arellano JB, Psencik J, Borrego CM, Ma YZ, Guyoneaud R, Garcia-Gil J, Gillbro T (2000) Effect of carotenoid biosynthesis inhibition on the chlorosome organization in *Chlorobium phaeobacteroides* strain CL1401. Photochem Photobiol 71:715–723

Arellano JB, Melo TB, Fyfe PK, Cogdell RJ, Naqvi KR (2004) Multichannel flash spectroscopy of the reaction centers of wild-

type and mutant *Rhodobacter sphaeroides*: bacteriochlorophyll$_B$-mediated interaction between the carotenoids triplet and the special pair. Photochem Photobiol 79:68–75

Balaban TS (2005) Tailoring porphyrins and chlorins for self-assembly in biomimetic artificial antenna systems. Acc Chem Res 38:612–623

Balaban TS, Tamiaki H, Holzwarth AR (2005) Chlorins programmed for self-assembly. Top Curr Chem 258:1–38

Billsten HH, Herek JL, Garcia-Asua G, Hashoj L, Polivka T, Hunter CN, Sundstrom V (2002) Dynamics of energy transfer from lycopene to bacteriochlorophyll in genetically-modified LH2 complexes of *Rhodobacter sphaeroides*. Biochemistry 41: 4127–4136

Blankenship RE, Matsuura K (2003) Antenna complexes from green photosynthetic bacteria. In: Green BR, Parson WW (eds) Light-harvesting antennas in photosynthesis. Kluwer Academic Publishers, Dordrecht, pp 195–217

Bryant DA, Vassilieva EV, Frigaard NU, Li H (2002) Selective protein extraction from *Chlorobium tepidum* chlorosomes using detergents. Evidence that CsmA forms multimers and binds bacteriochlorophyll *a*. Biochemistry 41:14403–14411

Chabera P, Fuciman M, Naqvi KR, Polivka T (2010) Ultrafast dynamics of hydrophilic carbonyl carotenoids—relation between structure and excited-state properties in polar solvents. Chem Phys 373:56–64

Christensson N, Polivka T, Yartsev A, Pullerits T (2009) Photon echo spectroscopy reveals structure-dynamics relationships in carotenoids. Phys Rev B 79, 245118

Frigaard NU, Bryant DA (2006) Chlorosomes: antenna organelles in photosynthetic green bacteria. In: Shively JM (ed) Complex intracellular structures in prokaryotes (series: Microbiology Monographs, vol. 2), pp 79–114. Springer, Berlin

Frigaard NU, Takaichi S, Hirota M, Shimada K, Matsuura K (1997) Quinones in chlorosomes of green sulfur bacteria and their role in the redox-dependent fluorescence studied in chlorosome-like bacteriochlorophyll *c* aggregates. Arch Microbiol 167:343–349

Ganapathy S, Oostergetel GT, Wawrzyniak PK, Reus M, Chew AGM, Buda F, Boekema EJ, Bryant DA, Holzwarth AR, de Groot HJM (2009) Alternating *syn-anti* bacteriochlorophylls form concentric helical nanotubes in chlorosomes. Proc Natl Acad Sci 106:8525–8530

Gradinaru CC, Kennis JTM, Papagiannakis E, van Stokkum IHM, Cogdell RJ, Fleming GR, Niederman RA, van Grondelle R (2001) An unusual pathway of excitation energy deactivation in carotenoids: singlet-to-triplet conversion on an ultrafast timescale in a photosynthetic antenna. Proc Natl Acad Sci 98:2364–2369

Hildebrandt P, Tamiaki H, Holzwarth AR, Schaffner K (1994) Resonance Raman-spectroscopic study of metallochlorin aggregates Implications for the supramolecular structure in chlorosomal BChl *c* antennae of green bacteria. J Phys Chem 98:2192–2197

Hirota M, Moriyama T, Shimada K, Miller M, Olson JM, Matsuura K (1992) High degree of organization of bacteriochlorophyll *c* in chlorosome-like aggregates spontaneously assembled in aqueous solution. Biochim Biophys Acta 1099:271–274

Ilagan RP, Christensen RL, Chapp TW, Gibson GN, Pascher T, Polivka T, Frank HA (2005) Femtosecond time-resolved absorption spectroscopy of astaxanthin in solution and in alpha-crustacyanin. J Phys Chem A 109:3120–3127

Klinger P, Arellano JB, Vacha FE, Hala J, Psencik J (2004) Effect of carotenoids and monogalactosyl diglyceride on bacteriochlorophyll *c* aggregates in aqueous buffer: implications for the self-assembly of chlorosomes. Photochem Photobiol 80:572–578

Kopczynski M, Lenzer T, Oum K, Seehusen J, Seidel MT, Ushakov VG (2005) Ultrafast transient lens spectroscopy of various C-40 carotenoids: lycopene, beta-carotene, (3R,3′ R)- zeaxanthin, (3R,3′ R,6′ R)-lutein, echinenone, canthaxanthin, and astaxanthin. Phys Chem Chem Phys 7:2793–2803

Latimer P, Eubanks CAH (1962) Absorption spectrophotometry of turbid suspensions—a method of correcting for large systematic distortions. Arch Biochem Biophys 98:274–285

Melo TB, Frigaard NU, Matsuura K, Naqvi KR (2000) Electronic energy transfer involving carotenoid pigments in chlorosomes of two green bacteria: *Chlorobium tepidum* and *Chloroflexus aurantiacus*. Spectrochim Acta A Mol Biol Spectrosc 56:2001–2010

Miyatake T, Tamiaki H (2005) Self-aggregates of bacteriochlorophylls-*c*, *d* and *e* in a light-harvesting antenna system of green photosynthetic bacteria: effect of stereochemistry at the chiral 3-(1-hydroxyethyl) group on the supramolecular arrangement of chlorophyllous pigments. J Photoch Photobio C 6:89–107

Miyatake T, Tamiaki H (2010) Self-aggregates of natural chlorophylls and their synthetic analogs in aqueous media for making light-harvesting systems. Coord Chem Rev 254:2593–2602

Montano GA, Wu HM, Lin S, Brune DC, Blankenship RE (2003) Isolation and characterization of the B798 light-harvesting baseplate from the chlorosomes of *Chloroflexus aurantiacus*. Biochemistry 42:10246–10251

Oostergetel GT, Reus M, Gomez Maqueo Chew A, Bryant DA, Boekema EJ, Holzwarth AR (2007) Long-range organization of bacteriochlorophyll in chlorosomes of *Chlorobium tepidum* investigated by cryo-electron microscopy. FEBS Lett 581:5435–5439

Oostergetel GT, van Amerongen H, Boekema EJ (2010) The chlorosome: a prototype for efficient light-harvesting in photosynthesis. Photosynth Res 104:245–255

Papagiannakis E, van Stokkum IHM, van Grondelle R, Niederman RA, Zigmantas D, Sundstrom V, Polivka T (2003) A near-infrared transient absorption study of the excited-state dynamics of the carotenoid spirilloxanthin in solution and in the LH1 complex of *Rhodospirillum rubrum*. J Phys Chem B 107:11216–11223

Pedersen MO, Underhaug J, Dittmer J, Miller M, Nielsen NC (2008) The three-dimensional structure of CsmA: a small antenna protein from the green sulfur bacterium *Chlorobium tepidum*. FEBS Lett 582:2869–2874

Polivka T, Frank HA (2010) Molecular factors controlling photosynthetic light-harvesting by carotenoids. Acc Chem Res 43:1125–1134

Psencik J, Ma YZ, Arellano JB, Garcia-Gil J, Holzwarth AR, Gillbro T (2002) Excitation energy transfer in chlorosomes of *Chlorobium phaeobacteroides* strain CL1401: the role of carotenoids. Photosynth Res 71:5–18

Psencik J, Ma YZ, Arellano JB, Hala J, Gillbro T (2003) Excitation energy transfer dynamics and excited-state structure in chlorosomes of *Chlorobium phaeobacteroides*. Biophys J 84:1161–1179

Psencik J, Ikonen TP, Laurinmäki P, Merckel MC, Butcher SJ, Serimaa RE, Tuma R (2004) Lamellar organization of pigments in chlorosomes, the light-harvesting complexes of green photosynthetic bacteria. Biophys J 87:1165–1172

Psencik J, Arellano JB, Ikonen TP, Borrego CM, Laurinmäki PA, Butcher SJ, Serimaa RE, Tuma R (2006) Internal structure of chlorosomes from brown-colored *Chlorobium* species and the role of carotenoids in their assembly. Biophys J 91:1433–1440

Psencik J, Collins AM, Liljeroos L, Torkkeli M, Laurinmäki P, Ansink HM, Ikonen TP, Serimaa RE, Blankenship RE, Tuma R, Butcher SJ (2009) Structure of chlorosomes from the green filamentous bacterium *Chloroflexus aurantiacus*. J Bacteriol 191:6701–6708

Sakuragi Y, Frigaard NU, Shimada K, Matsuura K (1999) Association of bacteriochlorophyll *a* with the CsmA protein in chlorosomes

of the photosynthetic green filamentous bacterium *Chloroflexus aurantiacus*. BBA-Bioenergetics 1413:172–180

Sorensen PG, Cox RP, Miller M (2008) Chlorosome lipids from *Chlorobium tepidum*: characterization and quantification of polar lipids and wax esters. Photosynth Res 95:191–196

Stanier RY, Smith JHC (1960) The chlorophylls of green bacteria. Biochim Biophys Acta 41:478–484

Steensgaard DB, Wackerbarth H, Hildebrandt P, Holzwarth AR (2000) Diastereoselective control of bacteriochlorophyll *e* aggregation. 3(1)-S-BChl *e* is essential for the formation of chlorosome-like aggregates. J Phys Chem B 104:10379–10386

Takaichi S, Wang ZY, Umetsu M, Nozawa T, Shimada K, Madigan MT (1997) New carotenoids from the thermophilic green sulfur bacterium *Chlorobium tepidum*: 1′,2′-dihydro-gamma-carotene, 1′,2′-dihydrochlorobactene, and OH-chlorobactene glucoside ester, and the carotenoid composition of different strains. Arch Microbiol 168:270–276

Uehara K, Mimuro M, Ozaki Y, Olson JM (1994) The formation and characterization of the in vitro polymeric aggregates of bacteriochlorophyll *c* homologs from *Chlorobium limicola* in aqueous suspension in the presence of monogalactosyl diglyceride. Photosynth Res 41:235–243

Umetsu M, Seki R, Kadota T, Wang ZY, Adschiri T, Nozawa T (2003) Dynamic exchange properties of the antiparallel bacteriochlorophyll *c* dimers. J Phys Chem B 107:9876–9882

van Stokkum IHM, Larsen DS, van Grondelle R (2004) Global and target analysis of time-resolved spectra. BBA-Bioenergetics 1657:82–104

Weber S (1988) Determination of stabilised, added astaxanthin in fish feeds and premixes with HPLC. In: Keller HE (ed) Analytical methods for vitamins and carotenoids in feeds, pp 59–61. Roche Publication No. 2264, Basel

Zupcanova A, Arellano JB, Bina D, Kopecky J, Psencik J, Vacha F (2008) The length of esterifying alcohol affects the aggregation properties of chlorosomal bacteriochlorophylls. Photochem Photobiol 84:1187–1194